Superlattices and Microstructures 140 (2020) 106468

Contents lists available at ScienceDirect

Superlattices and Microstructures

journal homepage: www.elsevier.com/locate/superlattices

Investigating the impact of layer properties on the performance of p-graphene/$CH_3NH_3PbI_3$/n-cSi solar cell using numerical modelling

Gagandeep [a], Mukhtiyar Singh [b], Ramesh Kumar [a,*], Vinamrita Singh [c]

[a] Department of Physics, Guru Jambheshwar University of Science & Technology, Hisar, India
[b] Department of Applied Physics, Delhi Technological University, Delhi, India
[c] Department of Applied Sciences and Humanities, Ambedkar Institute of Advanced Communication Technologies & Research, Delhi, India

ARTICLE INFO

Keywords:
AFORS-HET software
Perovskite solar cell
Graphene
Silicon
Power conversion efficiency

ABSTRACT

The use of multilayer p-graphene as hole transporting layer has been successfully shown to improve the performance of perovskite solar cell. The structure of p-graphene/$CH_3NH_3PbI_3$/n-cSi is designed and simulated in AFORS-HET software. We optimized the parameters of single layer p-graphene and obtained power conversion efficiency (PCE) of 12.21% under an illumination of AM 1.5G. With an increase in the number of p-graphene layers, the PCE falls down to 10.01%. The optimization of active layer parameters increases the PCE up to 12.27%. Further optimization of n-cSi parameters lead to the highest PCE of 16.75%. A significant effect of the operating temperature on the solar cell performance is observed. The effect of textured front surface on the solar cell performance is also studied and a PCE of 17.90% is obtained for textured surface as compared to 16.75% for planar surface. Our studies indicated that p-graphene may act as an efficient hole transporting layer in perovskite solar cell.

1. Introduction

The organic-inorganic hybrid perovskite solar cells (PSCs) have received great attention over the recent years because of its tuneable band gap and high absorption coefficient that produce large PCE [1–5]. A typical structure of PSC consists of the perovskite layer sandwiched between an electron transporting layer (ETL) and a hole transporting layer (HTL) along with front and back contacts. The ETL materials are used to extract and transport the electrons from the perovskite layer to the corresponding electrode. TiO_2 is a widely used ETL material for PSCs. However, TiO_2 material has some disadvantages such as intrinsic low mobility and production of deep traps by ultraviolet light, which results in charge accumulation, recombination in this layer and numerous current-voltage hysteresis [6–10]. The holes generated in perovskite layer are extracted and transported by the HTL materials which are broadly classified into two types i.e. one is organic HTL and the other is inorganic HTL. These HTL materials are selected based on their HOMO level, optical properties along with its doping ability. The organic HTL 2, 2′, 7, 7’ - tetrakis (N, N-DI-P-methoxypheny-amine)- 9,9’ - spirobifluorene (spiro-MeOTAD) is used for achieving large PCE [11]. The poly (3,4- ethylenedioxythiophene): polystyrene sulfonate (PEDOT: PSS) has also been employed as HTL in PSCs [12]. In contrast to the more expensive organic HTL materials, the inorganic HTL materials such as transition metal oxides NiO_x [13,14], CuO_x [15,16] and CrO_x [17,18] also established widespread interest.

* Corresponding author.
E-mail address: rameshkumar.bibiyan@gmail.com (R. Kumar).

https://doi.org/10.1016/j.spmi.2020.106468
Received 22 April 2019; Received in revised form 24 February 2020; Accepted 25 February 2020
Available online 2 March 2020

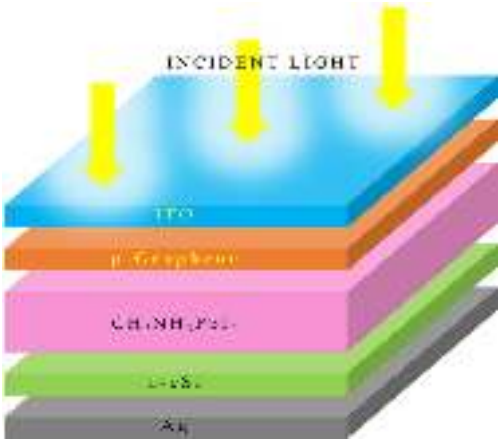

Fig. 1. Simulated hybrid PSC structure.

Recently, it has been observed that graphene with its exceptional properties have positive impact on the development of PSCs. The low-cost graphene with its high carrier mobility (2×10^5 $cm^2/V{\cdot}s$) [19], large optical transparency [20], large thermal conductivity [21], and high melting point [22] can be employed either as HTL or ETL, or both, at the electrodes in PSCs. Watanabe et al. [23] studied the PSC by introducing the graphene as HTL in place of spiro-OMeTAD and obtained an efficiency of 7.1% with J_{sc} of 21.3 mA/cm^2.

They also compared the two PSC structures, i.e., FTO/TiO_2/$CH_3NH_3PbI_3$/graphene/Au and FTO/TiO_2/$CH_3NH_3PbI_3$/spiro-OMeTAD/Au. They found that the PSC structure based on graphene as HTL is more stable as compared to spiro-OMeTAD based PSC. The authors also suggested that the PSC performance may be improved by changing the work function of graphene and proposed doping as an approach to modify the work function of the graphene. Cao et al. [24] introduced functionalized nano-graphene (perthiolated-trisulfur-annulated hexa-peri-hexabenzocoronene,TSHBC) as HTL in PSC which accelerated the hole transportation rate. The authors obtained an efficiency of 12.81% with the device structure of FTO/TiO_2/$CH_3NH_3PbI_3$/TSHBC/Au. They also suggested that graphene has better stability as compared to spiro-OMeTAD and the device fabrication can be finished with 45% humidity in air, while this condition is not suitable for spiro-OMeTAD. The hole-transportation can be improved by introducing extra graphene into TSHBC and the PSC reached an efficiency of 14%. Yan et al. [25] reported that the hole extraction rate for multilayer and single layer graphene is 5.1 and 3.7 ns^{-1}, respectively and obtained an efficiency of 11.5% with multilayer graphene. According to the findings of the authors, a Schottky barrier is formed at the perovskite/graphene interface and an increase in the hole transportation and extraction rate is achieved by decreasing the recombination rate as well as blocking the electrons.

Moreover, graphene has been used as an additive in ZnO and TiO_2 based ETLs, and showed an increase in efficiency [26,27]. Wang et al. [27] further compared different PSC structures with TiO_2 ETL, graphene only ETL, without ETL and high temperature sintered TiO_2 ETL. They found that the highest efficiency was achieved for the cell with TiO_2 + graphene as an ETL, but nonetheless, graphene-based PSC showed better results when compared to the cell without an ETL. This demonstrates that graphene is a suitable ETL for PSCs, and the PCE and life time of solar cell devices could thus be increased using graphene as a buffer layer.

The PSCs using p-Si as an inorganic HTL have been previously modelled [28], and it has been further indicated that p-Si has good chemical stability, low cost and higher hole mobility [29]. Yan et al. [30] also studied a low-cost Si-nanowire/perovskite hybrid solar cell and obtained a PCE of 13.3%.Therefore, PSCs with n-cSi (crystalline silicon) layer may also be modelled to investigate its role as an efficient ETL.

Having the above observations in mind, the PSCs performance can be upgraded by inserting the perovskite layer in between the graphene and Si layers. In the present work, we designed the following configuration p-graphene/$CH_3NH_3PbI_3$/n-cSi for hybrid solar cell using AFORS-HET (Automat for Simulation of Heterostructures) software [31–33]. We optimized each layer and obtained the parameters for highest efficiency. The impact of operating temperature and textured front surface on the performance of the solar cell is also examined. Our findings indicate that p-graphene and n-cSi can act as an efficient HTL and ETL, respectively, in PSC and promising hybrid solar cells may be achieved with superior performance.

2. Simulating structure

To realize the idea related to the usage of graphene as HTL material, we used a theoretical approach to study hybrid PSCs with silicon layer. We designed a p-i-n based structure as p-graphene/$CH_3NH_3PbI_3$/n-cSi, with ITO (indium tin oxide) and Ag (silver) as the front and back contacts in AFORS-HET software. AFORS-HET uses the one-dimensional semiconductor equations related to Shockley Reed Hall statistics solver and Lambert-Beer law for optical parameters of different photovoltaic devices. The complete PSC configuration is ITO (80 nm)/p-graphene (0.334–6.68 nm)/$CH_3NH_3PbI_3$ (50–1000 nm)/n-cSi (50–300 μm)/Ag (0.001 cm) as shown in Fig. 1. Here, the light enters through the graphene layer and generates electron-hole pairs in the active layer. The generated electrons/holes are collected and transferred by n-cSi and p-graphene to the respective electrodes. We optimized various parameters such as layer thickness, electron affinity (χ), energy band gap (E_g), dielectric constant (dk), doping concentrations (N_D/N_A), effective conduction/

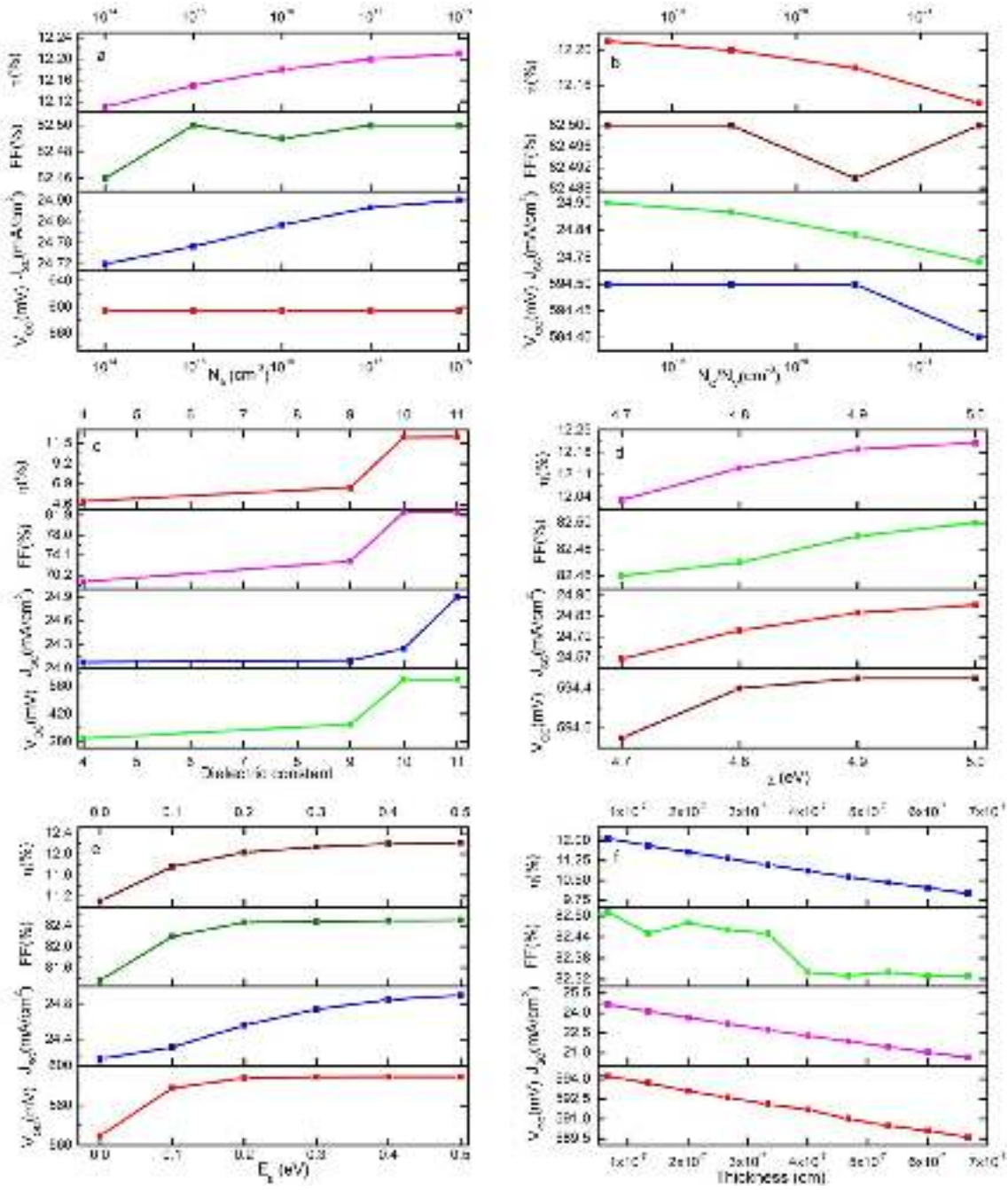

Fig. 2. PSC performance with the p-graphene parameters (a) N_A (cm^{-3}), (b) N_C/N_V (cm^{-3}), (c) dielectric constant (dk), (d) electron affinity (χ) (eV), (e) energy band gap E_g (eV) and (f) thickness, where the value of perovskite and n-cSi parameters used were: $N_C/N_V = 2.5 \times 10^{20}$ cm^{-3} and 3×10^{19} cm^{-3}, $N_D = 2 \times 10^{14}$ cm^{-3} and 1×10^{16} cm^{-3}, $E_g = 1.5$ eV and 1.12 eV, $\chi = 3.9$ eV and 4.05 eV, dk = 30 and 11.9, and thickness = 50 nm and 100 μm, respectively.

valence band density (N_C/N_V) to observe the effect on the PCE (η), open circuit voltage (V_{oc}), fill factor (FF) and current density (J_{sc}) of PSC. The simulation parameters used in the software are taken from different experimental and theoretical reports [34–40].

To increase the efficiency of solar cells, the front contact surface can be made textured. This textured surface reduces light reflection; assists in light trapping and consequently may increase the overall device efficiency due to increase in current. In this work, both non-textured and textured front contacts have been applied to model the solar cell performance.

Table 1
Summary of the optimized parameters used in simulation.

Optimized parameters	HTL(p-graphene)	Absorber layer($CH_3NH_3PbI_3$)	ETL(n-cSi)
Thickness(cm)	3.34×10^{-8}	5×10^{-6}	0.03
dk	11	6.5	11.9
$N_A(cm^{-3})$	1×10^{18}	1×10^{13}	–
$N_D(cm^{-3})$	–	1×10^{13}	1×10^{17}
$N_C(cm^{-3})$	3×10^{18}	2.5×10^{20}	3×10^{19}
$N_V(cm^{-3})$	3×10^{18}	2.5×10^{20}	3×10^{19}
μ_e ($cm^2V^{-1}s^{-1}$)	1×10^5	50	1350
μ_h ($cm^2V^{-1}s^{-1}$)	10	50	450
χ (eV)	5.0	3.9	4.4
E_g(eV)	0.5	1.5	1.12

3. Results and discussions

3.1. Optimization of p-graphene layer

The graphene can be made p-type material by doping with trivalent atoms like boron with the help of different techniques such as thermal annealing, ball milling, liquid, solid and gaseous phase chemical doping, and in-situ doping during chemical vapour deposition (CVD) [41,42]. The heteroatom doping onto a graphene sheet can influence the chemical, physical, electronic and photonic properties of the material. The solar cell parameter optimization was started by varying the parameters of p-graphene layer first, and taking some initial values of the perovskite and n-cSi layers. The values of perovskite layer parameters were fixed at $N_A = 3 \times 10^{14}$ cm^{-3}, $N_C/N_V = 2.5 \times 10^{20}$ cm^{-3}, $E_g = 1.5$ eV, $\chi = 3.9$ eV, dk = 30 and thickness = 50 nm. The n-cSi parameters used were $N_D = 1 \times 10^{16}$ cm^{-3}, $N_C/N_V = 3 \times 10^{19}$ cm^{-3}, $E_g = 1.12$ eV, $\chi = 4.05$ eV, dk = 11.9 and thickness = 100 μm. The p-graphene layer parameters kept at constant values were $N_C/N_V = 3 \times 10^{18}$ cm^{-3}, $E_g = 0.5$ eV, $\chi = 5.0$ eV, dk = 11 and thickness 0.334 nm. We varied the acceptor concentration (N_A) of the p-graphene layer from 1×10^{14} to 1×10^{18} cm^{-3} and observed its effect on PSC parameters. The variation of solar cell parameters with N_A is mentioned in Fig. 2(a). From the figure, it is observed that as N_A increases from 1×10^{14} to $1 \times 10^{18}cm^{-3}$, the J_{sc} varies from 24.72 mA/cm^2 to 24.90 mA/cm^2,V_{oc} remains constant, PCE changes from 12.11% to 12.21%, and FF varies from 82.46% to 82.50%. As we increase the acceptor concentration in graphene sheet, the graphene work function is lowered, and the conductivity rises. This leads to an increase in J_{sc}, PCE and FF, but the V_{oc} does not change. Next, the parameters N_C and N_V are changed from 3×10^{18} to 3×10^{21} cm^{-3} for the monolayer graphene and the simulated results are given in Fig. 2(b). Again, the V_{oc} remained constant, but J_{sc} reduced from 24.90 mA/cm^2 to 24.77 mA/cm^2, FF slightly changes from 82.50% to 81.49% and the overall efficiency also changed from 12.21% to 12.14% with increase in N_C/N_V value. The minority charge carrier density decreases as N_C/N_V is increased because of trapping of free carrier charges and small life time of photo induced carriers. The V_{oc} reduces from 594.50 mV to 594.40 mV beyond $\sim 5 \times 10^{20}$ cm^{-3} as such high values of N_C/N_V reduces the barrier height and the built-in voltage [43]. Thus, reducing N_C/N_V below 10^{19} cm^{-3} gives high overall PCE. In both the cases of varying N_A and N_C/N_V, it is found that significant changes in the solar cell parameters are not observed in the range under study. This implies that the acceptor concentration and the band densities do not affect the charge transport to a great extent in this case.

The dielectric constant (dk) of p-graphene layer was varied keeping other parameters constant as given in Fig. 2(c). The dk value for single layer graphene is reported in between 4 and 11 [44]. The maximum value of all the solar cell parameters is obtained at dk = 11 and the maximum values of V_{oc}, J_{sc}, FF and PCE are 594.50 mV, 24.90 mA/cm^2, 82.50% and 12.21% respectively. The electron affinity values of p-graphene vary in the range 4.7–5 eV. The observations presented in Fig. 2(d) reveal that the PCE of the simulated cell is increased from 12.03% to 12.21%, being maximum at 5 eV, because on increasing the electron affinity, the barrier height is increased which impedes the flow of electrons towards ITO leading to lesser recombination and results in rising J_{sc} from 24.56 mA/$cm^2$to 24.90 mA/cm^2. Thus, high electron affinity is useful for increasing the device efficiency. This is also in agreement with other reports where high electron affinity materials are shown to be preferable for HTL [45]. The change in the overall efficiency is low with change in electron affinity because even with the starting value of $\chi = 4.7$, the barrier height between the HTL/perovskite interface is appropriate for hole extraction.

Some studies [34,43] showed that graphene has a band gap that varies from 0 to 0.25 eV, whereas, Nevis et al. [35] have reported that graphene has a band gap of 0.5 eV. In view of these studies, we varied the energy gap of graphene from 0 to 0.5 eV as depicted in Fig. 2(e). The PCE increases from 11.11% to 12.21%, J_{sc} changes from 24.18 mA/cm^2 to 24.90 mA/cm^2 and V_{oc} rises from 564.70 mV to 594.50 mV with increase in the energy band gap of graphene. The band gap of graphene affects the built-in potential which may have caused the observed increase in V_{oc}. Only a small change in J_{sc} is observed since it is governed by the production of photocurrent in the active layer and not the band gap of the HTL. Moreover, a greater barrier at the interface between HTL and perovskite layer sufficiently separates the electron hole pair aiding in an increase in current. Consequently, the FF and PCE increases primarily due to increase in V_{oc}, but tends to saturate fast at high band gap.

The impact of number of graphene layers on solar cell performance is also investigated. The number of graphene layers directly influences the sheet resistance as well as the optical transparency. The sheet resistance and optical transparency is reduced with increase in the graphene layers. To prove this concept, the number of graphene layers is varied up to 20 layers. The highest efficiency 12.21% is obtained for single layer graphene having thickness of 0.334 nm. As we increase the number of graphene layers the

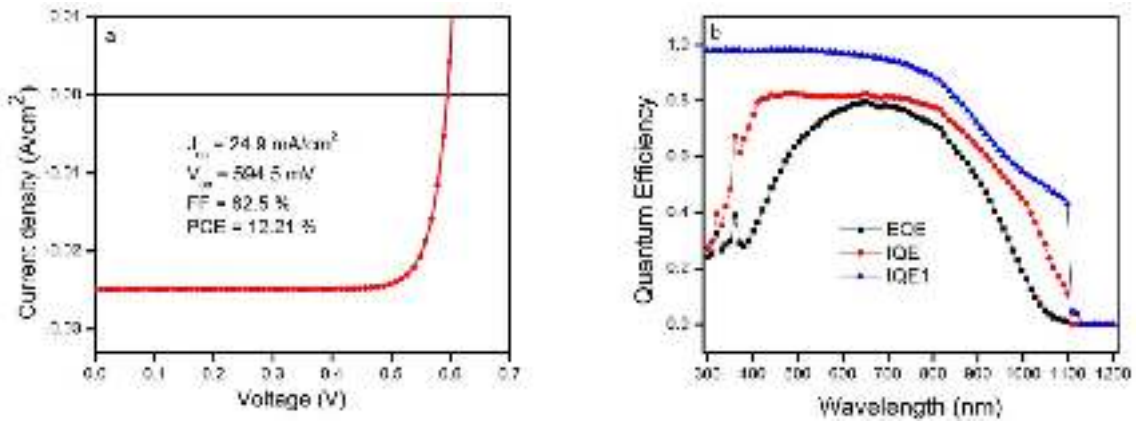

Fig. 3. (a) Current density-voltage curve for p-graphene optimized thickness and (b) Quantum Efficiency with wavelength.

efficiency decreases to 10.01%, while FF varies from 82.50% to 82.33%. The V_{oc} and J_{sc} also decrease from 594.50 mV to 589.60 mV and 24.90 mA/cm^{2}to 20.63 mA/cm^2, respectively, with the number of layers or increase in thickness of graphene layer. The parameter variations are shown in Fig. 2(f). The decrease in performance may be attributed to lesser light reaching the active layer lowering the photocurrent. The monolayer graphene shows an optical transparency of 97.7% which is further reduced with increase in graphene layers [46]. An addition of each layer reduces the transparency by 2.3%.

After optimization of graphene parameters, we were able to achieve the best-suited properties of graphene layer that can be employed as a HTL in PSC. The optimized parameters are tabulated in Table 1. The current density-voltage (J-V) characteristics and the quantum efficiency (QE) variation versus wavelength for optimized p-graphene layer are plotted in Fig. 3(a) and (b) respectively. The figures depict the J-V characteristics and QE of the cell using optimized value of p-graphene parameter only and with the initial values mentioned above for perovskite and n-cSi layers. For the simulated structure, quantum efficiency has been calculated in the range of 300–1200 nm under the illumination condition of 1×10^{16} cm^{-2}s^{-1} monochromatic intensity and 10 nm spectral widths. Here the external quantum efficiency (EQE) and internal quantum efficiency (IQE and IQE1) of the optimized cell have been given in Fig. 3(b). The EQE gives the ratio of the charge carriers collected by the solar cell to the total number of incident photons by the external source, regardless of whether the photons are absorbed, reflected or transmitted. On the other hand, the IQE considers only the photons absorbed by the solar cell but does not consider whether these absorbed photons contribute to the current or not. Thirdly, IQE1 further corrects the IQE by subtracting those photons which may be absorbed by the layers other than the active layer, i.e., the contact layers, and thereby, not contributing to the current. Due to this, the EQE is always less than the IQE and IQE1 as observed in Fig. 3(b) as well.

The IQE and EQE of the cell increase and reach a maximum value, and thereafter decrease with wavelength [39]. It may be interpreted from Fig. 3(b) that the IQE1 becomes almost unity in the wavelength range of 300–700 nm indicating that the photons absorbed by the perovskite layer contributes sufficiently to the output current. The IQE decreases for the whole wavelength range and is approximately 80% in the 400–800 nm range, implying significant absorption by the layers other than the perovskite layer. Further reduction in the quantum efficiency is found in EQE, suggesting a loss of incident photons. Thus, this points towards the need of device engineering so that improvement in the absorption of incident photons can be achieved by reducing the reflection losses.

3.2. Optimization of perovskite layer

After optimizing the p-graphene layer parameters, we optimized the perovskite layer parameters by using the values of p-graphene parameters as mentioned in Table 1 and keeping the n-cSi parameter values as given in section 3.1. The properties of the perovskite layer have been modified in order to obtain the largest PCE for this configuration. The dielectric constant (dk) of the active layer depicts the nature of Columbian forces among the electron-hole pairs and other charges in the material. The behaviour of solar cell characteristics with dk is shown in Fig. 4(a). From the figure it can be seen that the PCE of the device varies from 12.27% to 12.21% with dk varying from 6.5 to 30 [47,48]. The FF of the device remains constant with value 82.51%, for dk 6.5–25, and after this FF falls up to the value 82.50% for dk from 25 to 30. The open circuit voltage (V_{oc}) of the device remains constant with value 594.50 mV and J_{sc} varies from 25.01 mA/cm^2 to 24.90 mA/cm^2 under the dk variation from 6.5 to 30. The optimized value of dk = 6.5 is taken for further calculations.

After optimizing the dk, we varied the N_C/N_V within the range of 2.5×10^{18} to 2.5×10^{20} cm^{-3}. As we increase N_C/N_V the minority charge carrier density decreases. Consequently, V_{oc} was constant at value 594.70 mV, fill factor varied from 82.27% to 82.49% and J_{sc} varied from 24.99 mA/cm^2 to 25.01 mA/cm^2 while the efficiency changed slightly from 12.23% to 12.27% (Fig. 4(b)). Further, the N_A/N_D is changed in the range 1×10^{13} to 1×10^{17} cm^{-3}, and the simulated values in Fig. 4(c) illustrate that the defect states exist in the perovskite layer resulting a noticeable change in J_{sc} and efficiency value change from 12.27% to 12.01%.

The thickness of the absorbing layer plays a very important role in the working of the device. Keeping the optimized values of above-mentioned parameters for the absorbing layer, we varied the thickness of the active layer in the range 50–1000 nm [39]. With

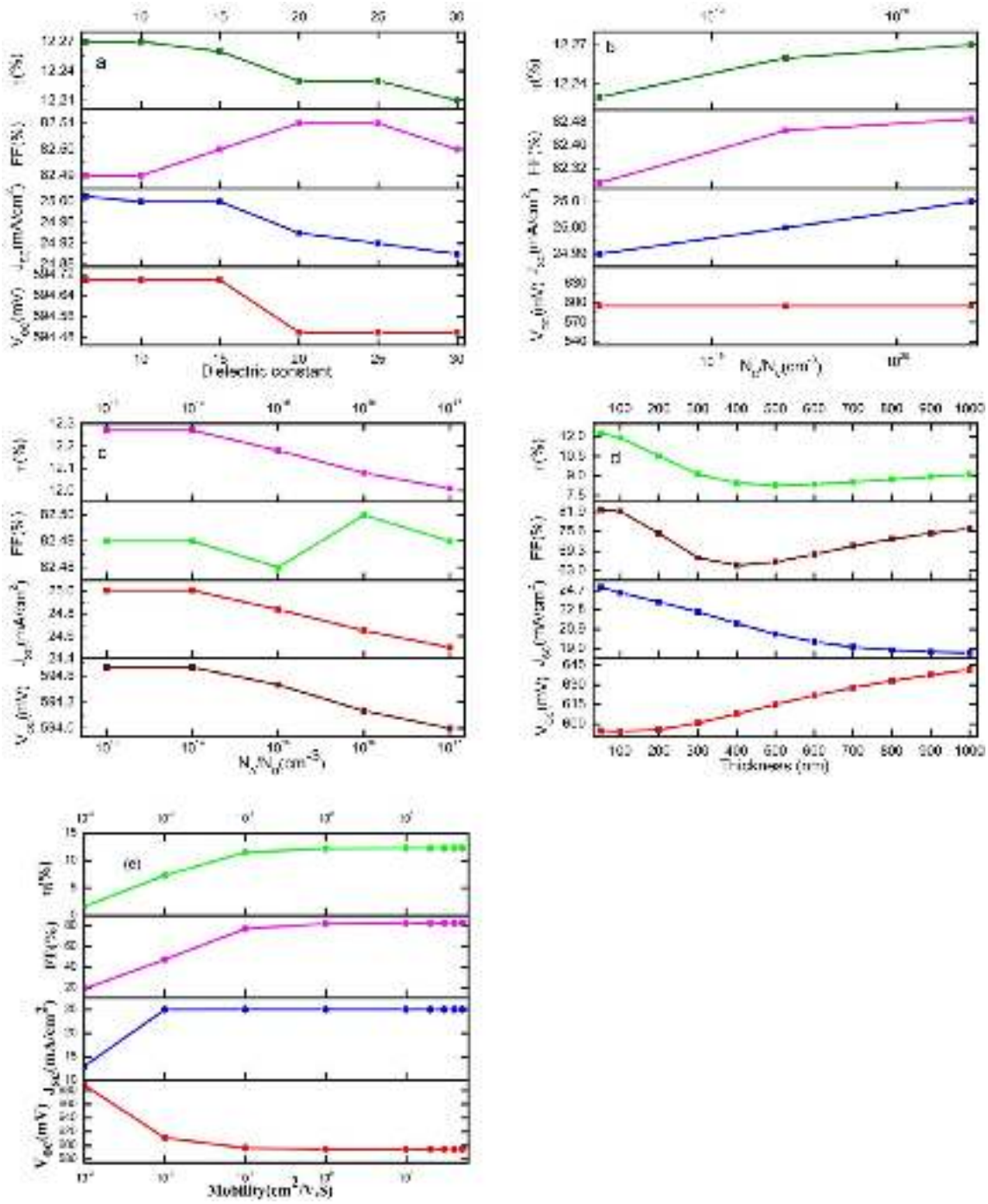

Fig. 4. PSC performance with perovskite parameters optimization (a) dk, (b) N_C/N_V (cm^{-3}), (c) N_A/N_D (cm^{-3}), (d) thickness (nm) and (e) mobility (μ_e/μ_h) (cm^2/Vs) where p-graphene and n-cSi parameters used were: $N_D = 0$ and 1×10^{16} cm^{-3}, $N_C/N_V = 3 \times 10^{18}$ and 3×10^{19} cm^{-3}, $E_g = 0.5$ eV and 1.12 eV, $\chi = 5$ and 4.05 eV, dk = 11 and 11.9, and thickness = 0.334 nm and 100 μm, respectively.

the increase in absorber thickness, the absorption of light in the layer also increases. The variation in PCE, FF, J_{sc} and V_{oc} with absorber layer thickness is shown in Fig. 4(d). The PCE and J_{sc} decreases from 12.27% to 9.11% and 25.01 mA/cm^2 to 18.57 mA/cm^2 respectively with thickness because a thicker layer may result into increased recombination and lower charge collection efficiency. Hence, using an optimum thickness would ensure a maximum current output from the device. The value of active layer thickness is taken around 50 nm in this case. After optimizing the thickness of the active layer, we varied the charge carrier mobility (μ_e/μ_h) in the range of 10^{-3} cm^2/V.s to 50 cm^2/V.s [49] and noted its effect on the performance of the cell. From Fig. 4(e) it is observed that all the

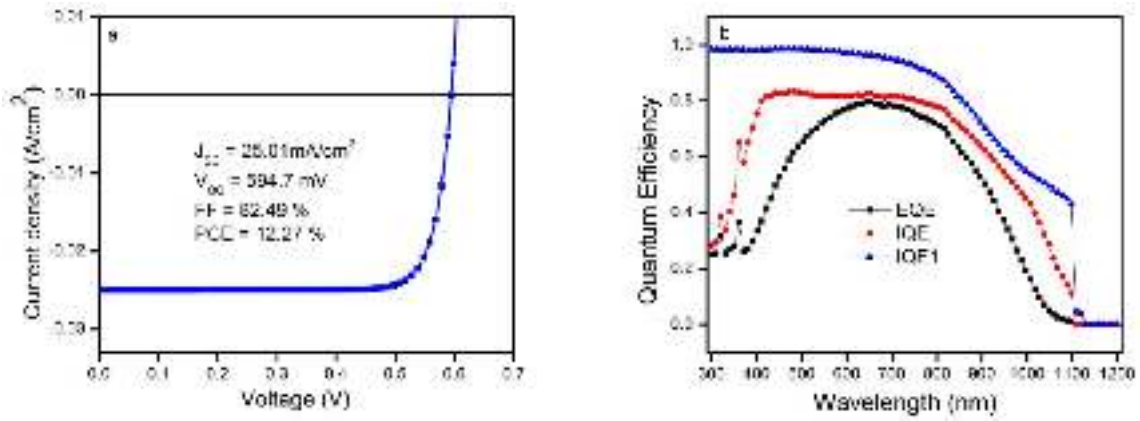

Fig. 5. (a) Current density-voltage curve for perovskite optimized thickness and (b) Quantum Efficiency with wavelength.

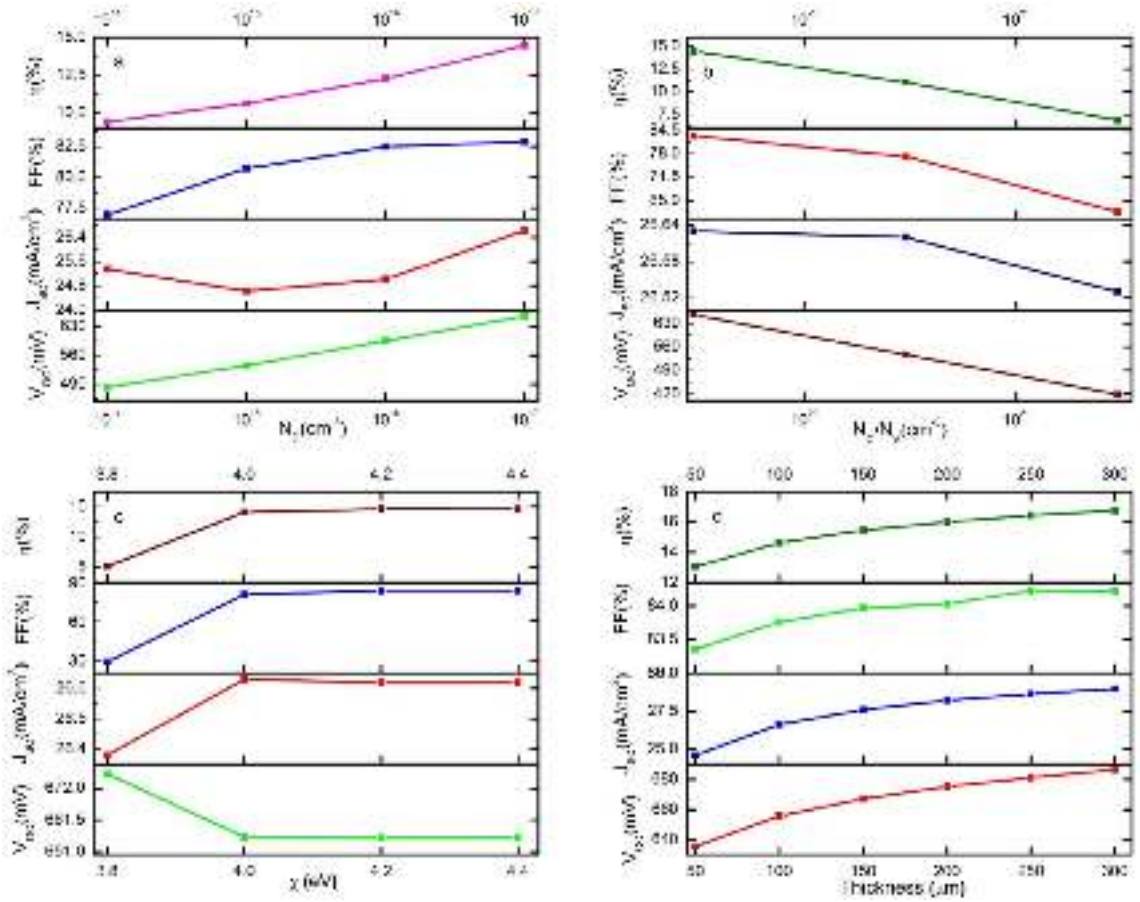

Fig. 6. PSC performance with the variation in n-cSi parameters, (a) N_D (cm^{-3}), (b) N_C/N_V (cm^{-3}), (c) χ (eV) and (d) thickness of n-cSi layer (μm) by considering the parameters of p-graphene and perovskite layers mentioned in Table 1.

parameters i.e., J_{sc}, FF and efficiency increase significantly up to 10 cm^2/V.s from the initial 13 mA/cm^2 to 25.01 mA/cm^2, 18.79%–82.48% and 1.68%–12.27% respectively, except V_{oc} with mobility and become almost constant up to 50 cm^2/V.s. This may be due to the decrease in recombination of charge carriers as a result of increase in mobility. The optimized parameters for the perovskite layer are summarized in Table 1. Thus, it may be stated that the thickness and mobility values of the perovskite layer dominantly affect the performance of the solar cell. On the other hand, the parameters like dielectric constant, N_C/N_V, N_A/N_D only slightly improve the performance of the solar cell. This may be because at the initial value of the perovskite thickness taken as 50 nm, the charge transport is

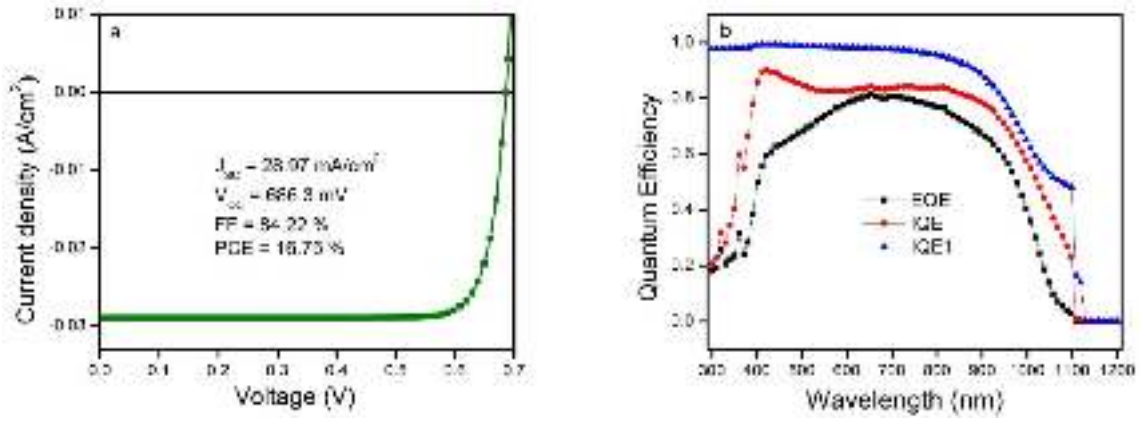

Fig. 7. (a) Current density-voltage curve for n-cSi optimized parameters and (b) Quantum Efficiency with wavelength.

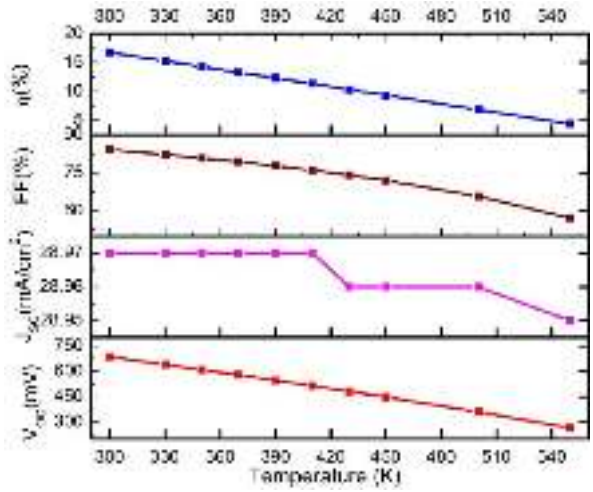

Fig. 8. PSC parameters variations with operating temperature.

adequate due to the long diffusion length of the perovskite material and the suitable built-in voltage at the HTL/perovskite interfaces, saturating the efficiency of the solar cell without much change in the parameter range under study. The solar cell J-V characteristics as well as quantum efficiency variation with wavelength for optimized parameters are plotted in Fig. 5(a) and (b). The behaviour of the cell is shown for the optimized value of perovskite layer and p-graphene parameters mentioned in Table 1, while the parameters for n-cSi mentioned in section 3.1 were used.

3.3. Optimization of n-crystalline silicon layer

For obtaining the best possible structure, layer parameters were optimized by considering the parameters of p-graphene and perovskite layers mentioned in Table 1. As, the donor concentration (N_D) in n-cSi is increased from 1×10^{14} to 1×10^{17} cm^{-3}, the work function of the ETL is increased, which results to an increase in V_{oc}. Thus, the values of the performance parameters of the device increased with increase in N_D and the results are shown in Fig. 6(a). Keeping $N_D = 1 \times 10^{17}$ cm^{-3}, the value of N_C/N_V was changed from of 3×10^{19} to 3×10^{21} cm^{-3} and the variation in the device performance is depicted in Fig. 6(b). From the graph it is seen that the V_{oc} significantly reduces from 655.70 mV to 419 mV, while J_{sc} decreased slightly from 26.63 mA/cm^2 to 26.53 mA/cm^2 with the variation in N_C/N_V. The efficiency is reduced to 6.89%. Then taking the values of $N_C/N_V = 3 \times 10^{19}$ cm^{-3} and $N_D = 1 \times 10^{17}$ cm^{-3}, we varied the electron affinity (χ) from 3.8 eV to 4.4 eV. In this range V_{oc} was found to change from 676.80 mV to 655.70 mV but J_{sc} decreased, FF and PCE of the cell increased initially and then remained constant as can be seen from Fig. 6(c). At $\chi = 4.2$ eV, the highest value of PCE was attained and have a value 14.62%. Next, the thickness of the n-cSi layer was varied from 50 μm to 300 μm and the changes are depicted in Fig. 6(d). The highest PCE is found to be 16.75% at a thickness of 300 μm. The simulation parameters are mentioned in Table 1. The J-V characteristics and the QE for optimized thickness of n-cSi are plotted in Fig. 7(a and b) and confirm the PCE of 16.75% for this configuration.

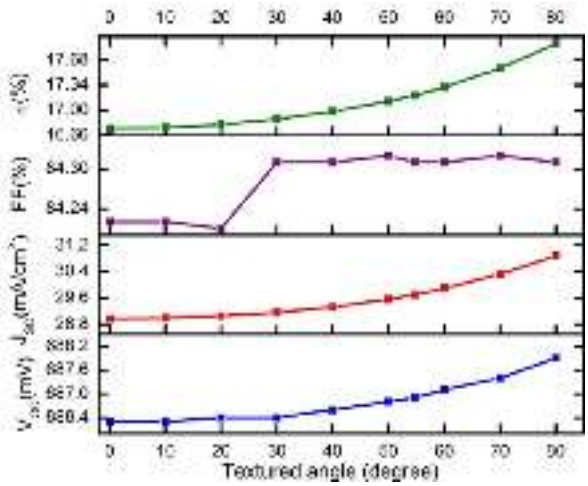

Fig. 9. PSC performance variation with textured front surface.

3.4. Influence of operating temperature on the PSC performance

The different layer parameters in heterojunction solar cell have been optimized to obtain the best possible efficiency of the device. To further understand the working of the device, the influence of operating temperature needs to be analysed. In the present study, we vary the temperature from 300 K to 550 K. The temperature change is taken as an external parameter in the simulation. As the temperature increases across the device, the energy band gap of the layer and carrier mobility across the layer interface is affected. The carrier recombination increases with the rise in temperature. The degradation in the values of performance parameters has also been previously attributed to the deformation and stress enhancement in device under the influence of temperature. These effects cause poor interconnectivity between the layers and create more interfacial defects. A high recombination rate prevails resulting into an increase in the series resistance and reduction in carrier diffusion length [50]. This is confirmed by our modelling results as depicted in Fig. 8. The highest PCE is obtained at 300 K and has a value of 16.75%.

3.5. Effect of textured surface on the PSC performance

The working of a device is also influenced by the nature of front contact surface i.e. whether the front contact is plane or textured. When the light falls on the front contact having textured surface with pyramidal topology, its angle of incidence with reference to the inclined surfaces of the pyramids is changed. The front textured surface not only reduces the reflection, but also in effect increases the optical path length as well as the optical thickness of the absorber. We simulated the PSC structure with and without textured front surface. The variations in solar cell parameters with the angle of inclination of the pyramidal texture, hence forth referred to as the angle of texture, are presented in Fig. 9. The PCE with textured surface is 17.90% as compared to 16.75% without textured surface. Here, we varied the angle of texture from 0° to 80°. The value of J_{sc} is increased from 28.97 mA/cm^2 to 30.87 mA/cm^2. This variation in J_{sc} is related to the optical confinement of the incident light due to multiple reflections; the short circuit current density being proportional to incident light. The value of V_{oc} increases from 686.3 mV to 687.9 mV with the angle of texture varying from 0° to 80°. The FF of the device also varies from 84.22% to 84.31%. This behaviour is due to the increased optical confinement with increase in the angle of textured surface.

The PCE of 17.90% for textured front surface is in good agreement with the other graphene based experimental studies [51] and also enhanced as compared to other Si/perovskite hybrid solar cell [30].

4. Conclusion

In the present study, we used p-graphene and n-cSi as a hole transporting material and electron transporting material respectively in the perovskite solar cell and simulated the structure using AFORS-HET software. We noticed the effect of different layers on the working of the device. The power conversion efficiency 16.75% is obtained for optimized structure. We studied the effect of operating temperature as well as textured surface of front contact on the device performance. The device parameters decrease with the rise in temperature. The efficiency for textured front surface is 17.90% as compared to 16.75% for plane front surface. This theoretical study shows that p-graphene and n-cSi can be used as an efficient HTL and ETL respectively in hybrid perovskite solar cell.

Authors Statement

All the authors equally contributed for the problem, mention in the manuscript.

Declaration of competing interest

The authors declared that they don't have any conflict of interest.

Acknowledgement

One of the authors (**Ramesh Kumar**) gratefully acknowledges the University Grants Commission **(**UGC**), INDIA** for the financial grant received through **START-**UP GRANT (No. F.30–364/2017 (BSR), Dated December 15, 2017). The authors are also thankful to Dr. Pawan K. Tyagi (Central University of Haryana) for fruitful discussion on AFORS-HET software.

Appendix A. Supplementary data

Supplementary data to this article can be found online at https://doi.org/10.1016/j.spmi.2020.106468.

References

[1] P. Gao, M. Gratzel, M.K. Nazeeruddin, Organohalide lead perovskites for photovoltaic applications, Energy Environ. Sci. 7 (2014) 2442–2443, https://doi.org/10.1039/C4EE00942H.
[2] M.A. Green, A. Ho-Baillie, H.J. Snaith, The emergence of perovskite solar cells, Natl. Photon 8 (2014) 506–514, https://doi.org/10.1038/nphoton.2014.134.
[3] N.G. Park, M. Gratzel, T. Miyasaka, K. Zhu, K. Emery, Towards stable and commercially Available perovskite solar cells, Nat, Energy 1 (2016) 16152.
[4] H.J. Snaith, Perovskites:The emergence of a new era for low-cost, high-efficiency solar cells, J. Phys. Chem. Lett. 4 (2013) 3623, https://doi.org/10.1021/jz4020162.
[5] Z. Xing, et al., Photovoltaic performance and stability of fullerene/cerium oxide double electron transport layer superior to single one in p-i-n perovskite solar cells, J. Power Sources 389 (2018) 13–19, https://doi.org/10.1016/j.jpowsour.2018.03.079.
[6] H.-S. Kim, I. Mora-Sero, V. Gonzalez-Pedro, F. Fabregat-Santiago, E.J. Juarez-Perez, N.-G. Park, J. Bisquert, Mechanism of carrier accumulation in perovskite thin absorber Solar cells, Nat. Commun. Now. 4 (2013) 2242, https://doi.org/10.1038/ncomms3242.
[7] H.J. Snaith, A. Abate, J.M. Ball, G.E. Eperon, T. Leijtens, N.K. Noel, S.D. Stranks, J, T.-W. Wang, K. Wojciechowski, W. Zhang, Anomalous hysteresis in perovskite solar cells, J. Phys. Chem. Lett. 5 (2014) 1511–1515, https://doi.org/10.1021/jz500113x.
[8] T. Leijtens, G.E. Eperon, S. Pathak, A. Abate, M.M. Lee, H.J. Snaith, Overcoming ultraviolet light instability of sensitized TiO_2 with meso-super structured Organometal trihalide perovskite solar cells, Nat. Commun. 4 (2013) 2885, https://doi.org/10.1088/1361-6528/aa6956.
[9] S. Ito, S. Tanaka, K. Manabe, H. Nishino, Effects of surface blocking layer of Sb_2S_3 on nanocrystalline TiO_2 for $CH_3NH_3PbI_3$ perovskite solar cells, J. Phys. Chem. C (2014) 16995–17000, https://doi.org/10.1088/0957-4484/27/23/235404.
[10] H.-S. Kim, I.-H. Jang, N. Ahn, M. Choi, A. Guerrero, J. Bisquert, N.-G. Park, Control of I-V hysteresis in $CH_3NH_3PbI_3$ perovskite solar cell, J. Phys. Chem. Lett. 6 (2015) 4633–4639, https://doi.org/10.1021/acs.jpclett.5b02273.
[11] J.A. Christians, et al., Tailored interfaces of encapsulated perovskite solar cells for >1,000 hour operational stability, Nat. Energy 3 (2018) 6874, https://doi.org/10.1038/s41560-017-0067-y.
[12] W. Chen, L. Xu, X. Feng, J. Jie, Z. He, Metal acetylacetonate series inInterface Engineering for full low- temperature- processed, high –performance, and Stable planar perovskite solar cells with conversion efficiency over 16% on 1 cm^2Scale, Adv. Mater. 29 (2017), 1603923, https://doi.org/10.1002/adma.201603923.
[13] W. Nie, et al., Critical role of interface and crystallinity on the performance and photo stability of perovskite solar cell on nickel oxide, Adv. Mater. 30 (2018) 1703879, https://doi.org/10.1002/adma.201703879.
[14] W. Chen, et al., Efficient and stable large –area perovskite solar cells with inorganic Charge extraction layers, Science 350 (2015) 944–948, https://doi.org/10.1126/science.aad1015.
[15] B.A. Nejand, V. Ahmadi, S. Gharibzadeh, H.R. Shahverdi, Cuprous oxide as a potential low-cost hole-transport material for stable perovskite solar cells, ChemSusChem 1–2 (2016) 1–10, https://doi.org/10.1002/cssc.201501273.
[16] C. Zuo, L. ding, Solution –processed Cu_2O and CuO as hole transport materials for efficient perovskite solar cells, Small 11 (2015) 5528–5532, https://doi.org/10.1002/smll.201501330.
[17] P. Qin, Q. He, G. Yang, X. Yu, L. Xiong, G. Fang, Metal ions diffusion at heterojunction chromium oxide/$CH_3NH_3PbI_3$ Interface on the stability of perovskite solar cells, Surf. Interfaces 10 (2018) 93–99, https://doi.org/10.1016/j.surfin.2017.12.006.
[18] P.L. Qin, H.W. Lei, X.L. Xheng, Q. Liu, H. Tao, G. Yang, W.J. Ke, L.B. Xiong, M.C. Qin, X.Z. Zhao, et al., Copper-doped chromium oxide hole transporting layer for perovskite solar cells: interface engineering and performance improvement, Adv. Mater. Interfaces 3 (2016) 1500799, https://doi.org/10.1002/admi.201500799.
[19] K.I. Bolotin, K.J. Sikes, Z. Jiang, M. Klima, G. Fudenberg, J. Hone, P. Kim, H.L. Stormer, Ultrahigh electron mobility in suspended graphene, Solid State Commun. 146 (2008) 351–355, https://doi.org/10.1016/j.ssc.2008.02.024.
[20] M. Acik, et al., Unusual infrared-absorption mechanism in thermally reduced graphene oxide, Nat. Mater. 9 (2010) 840, https://doi.org/10.1038/nmat2858.
[21] A.A. Balandin, S. Ghosh, W. Bao, I. Calizo, D. Teweldebrhan, F. Miao, C.N. Lau, Superior thermal conductivity of single-layer graphene, Nano Lett. 8 (2008) 902–907, https://doi.org/10.1021/nl0731872.
[22] E. Ganz, A.B. Ganz, L. Yang, M. Dornfeld, The initial stages of melting of graphene between 4000 K and 6000k, Phys. Chem. Chem. Phys. 19 (2017) 3756–3762, https://doi.org/10.1039/c6cp06940a.
[23] S. Watanabe, et al., Development of perovskite solar cell using graphene as a hole transport layer and a blocking layer, in: 7th World Conference on Photovoltaic Energy Conversion (WCPEC) IEEE, 2018, https://doi.org/10.1109/pvsc.2018.8548290.
[24] et Cao, et al., Well-defined thiolated nanographene as hole- transporting material for efficient and stable perovskite solar cell, J. Am. Chem. Soc. 137 (2015) 10914–10917, https://doi.org/10.1021/jacs.5b06493.
[25] K. Yan, et al., High-performance graphene-based hole conductor-free perovskite solar cells: Schottky junction enhanced hole extraction and electron blocking, Small 11 (2015) 2269–2274, https://doi.org/10.1002/smll.201403348.
[26] P.S. Chandrasekhar, Graphene/ZnO nanocomposite as an electron transport layer for perovskite solar cells; the effect of graphene concentration on photovoltaic performance, RSC Adv. 7 (2017) 28610–28615, https://doi.org/10.1039/C7RA02036H.
[27] J.T. Wang, et al., Low temperature processed electron collection layers of graphene/TiO2 nanocomposites in thin film perovskite solar cell, Nano Lett. 14 (2014) 724–730, https://doi.org/10.1021/nl403997a.
[28] X. Rong, et al., Impact of metal electrode work function of CH3NH3PbI3/p-Si planar heterojunction perovskite solar cells, Sol. Energy 158 (2017) 424–431, https://doi.org/10.1016/j.solener.2017.08.050.
[29] A. Madan et. al., Electrical and Optical properties of amorphous Si:F:H alloy, Am. J. Physiol. Lung Cell Mol. Physiol. 278 (200) 259-277.
[30] X. Yan, et al., A high efficiency Si nanowire array/perovskite hybrid solar cell, Nanoscale Research Letters (2017), https://doi.org/10.1186/s11671-016-1785-y.

[31] R. Stangl, M. Kriegel, M. Schmidt, AFORS-HET, version 2.2, a numerical computer program for simulation of heterojunction solar cells and measurements, in: Proceedin of the WCPEC-4, Fourth World Conference on Photovoltaic Energy Conversion (Hawaii, USA), 2006, pp. 1350–1353.
[32] R. Stangl, J. Haschke, C. Leendertz, Numerical Simulation of Solar Cells and Solar Cell Characterization Methods: the Open-Source on Demand Program AFORS-HET. Solar Energy 432, 2010, https://doi.org/10.5772/8073.
[33] R. Varache, C. Leendertz, M.E. Gueunier-Farret, J. Haschke, D. Muñoz, L. Korte, Investigation of selective junctions using a newly developed tunnel current model for solar cell applications, 2015 for Solar Cell Applications, Sol. Energy Mater. Sol. Cell. 141 (2015) 14–23, https://doi.org/10.1016/j.solmat.2015.05.014.
[34] K. Patel, P.K. Tyagi, Multilayer graphene as a transparent conducting electrode in Silicon heterojunction solar cell, AIP Adv. 5 (2015), 077165, https://doi.org/10.1063/1.4927545.
[35] M.S. Nevius, et al., Semiconducting graphene from highly ordered substrate interactions 115 (2015) 13680, https://doi.org/10.1103/PhysRevLett.115.1368022.
[36] F. Giannazzo, S. Sonde, V. Raineri, Electronic Properties of Graphene Probed at the Nanoscale, Physics and Applications of Graphene Experiments, 2011, pp. 353–376, https://doi.org/10.5772/15258.
[37] S.D. Sarma, S. Adam, E.H. Hwang, E. Rossi, Electronic transport in two-dimensional graphene, Rev. Mod. Phys. 83 (2011) 407–470, https://doi.org/10.1103/RevModPhys.83.407.
[38] M. Mohammed, Z. Li, J. Cui, T. Chen, Junction investigation of graphene/silicon Schottky diodes, Nanoscale Res. Lett. 7 (2012) 30, https://doi.org/10.1186/1556-276X-7-3022.
[39] S.M. Iftiquar, J.S. Kim, J. Yi, Investigation of highly efficient methyl ammonium lead halide perovskite solar cell with non-textured front surface, Optik 148 (2017) 54–62, https://doi.org/10.1016/j.ijleo.2017.08.141.
[40] D. Liu, M.K. Gangishetty, T.L. Kelly, Effect of $CH_3NH_3PbI_3$ thickness on device efficiency in planar heterojunction perovskite solar cells, J. Mater. Chem. 2 (2014), https://doi.org/10.1039/c4ta02637c, 1987.
[41] J. Rafiee, et al., Wetting transparency of graphene, Nat. Mater. 11 (2012) 217–222, https://doi.org/10.1038/nmat3228.
[42] S. Das and J. Drucker, Nucleation and growth of single layer graphene on Electrodeposited Cu by cold wall chemical vapour deposition, Nanotechnology 105601, https://doi.org/10.1088/1361-6528/aa593b.
[43] K. Patel, P.K. Tyagi, P- type multilayer graphene as a highly efficient transparent conducting electrode in silicon heterojunction solar cells, Carbon 116 (2017) 744–752, https://doi.org/10.1016/j.carbon.2017.02.042.
[44] G. Pirruccio, L.M. Moreno, G. Lozano, J.G. Rivas, Coherent and broadband enhanced optical absorption in graphene, ACS Nano 7 (2013) 4810–4817, https://doi.org/10.1021/nn4012253.
[45] P. Ru, et al., High electron affinity enables fast hole extraction for efficient flexible inverted perovskite solar cells, Adv. Energy Mater. (2020) 1903487, https://doi.org/10.1002/aenm.201903487.
[46] R.R. Nair, P. Blake, A.N. Grigorenko, K.S. Novoselov, T.J. Booth, T. Stauber, N M, R. Peres, A.K. Geim, Fine structure constant defines visual transparency of graphene, Science 20 (2008) 1308, https://doi.org/10.1126/science.1156965.
[47] M. Hirasawa, T. Ishihara, T. Goto, K. Uchida, N. Miura, Magneto absorption of the lowest exciton in perovskite-type compound $(CH_3NH_3)PbI_3$, Physica B 201 (1994) 427–430, https://doi.org/10.1016/09214526.(94).911304.
[48] W.A. Labana, L. Etgara, Depleted hole conductor-free lead halide iodide heterojunction solar cell, Energy Environ. Sci. 6 (11) (2013) 3249, https://doi.org/10.1039/C3EE42282H.
[49] B. Maynard, et al., Electron and hole drift mobility measurements on methylammonium lead iodide perovskite solar cells, Appl. Phys. Lett. 108 (2016), 173505, https://doi.org/10.1063/1.4948344.
[50] S. Sajid, A.M. Elseman, J. Ji, S. Dou, D. Wei, H. Huang, P. Cui, W. Xi, L. Chu, Y. Li, B. Jiang, M. Li, Computational study of ternary devices: low cost, and high efficient planar perovskite solar cells, Nano-Micro Lett. 10 (2018) 51, https://doi.org/10.1007/s40820-018-.
[51] A. Agresti, et al., Graphene-perovskite solar cells exceeds 18% efficiency: a stability Study, Chemsus chem 9 (18) (2016) 2609–2619, https://doi.org/10.1002/cssc.201600942.